Non–Pauli Errors Can Be Efficiently Sampled in Qudit Surface Codes

Yue Ma, Michael Hanks, and M. S. Kim
QOLS, Blackett Laboratory, Imperial College London, London SW7 2AZ, United Kingdom

(Received 29 March 2023; revised 19 July 2023; accepted 20 October 2023; published 16 November 2023)

Surface codes are the most promising candidates for fault-tolerant quantum computation. Single qudit errors are typically modeled as Pauli operators, to which general errors are converted via randomizing methods. In this Letter, we quantify remaining correlations after syndrome measurement for a qudit 2D surface code subject to non–Pauli errors via loops on the lattice, using percolation theory. Below the error correction threshold, remaining correlations are sparse and locally constrained. Syndromes for qudit surface codes are therefore efficiently samplable for non–Pauli errors, independent of the exact forms of the error and decoder.

DOI: 10.1103/PhysRevLett.131.200602

Quantum error correction is an important element towards large-scale quantum computation [1–6]. Topological codes on a two-dimensional plane [7–14] such as the toric code and the surface code, are among the most widely studied codes, as they only involve local interaction of the quantum registers [14]. A variety of experiments have demonstrated the path towards building a qubit topological code [15–24]. Recent studies have shown computational advantages using d-dimensional qudit systems [25–28]. The 2D toric code and surface code have been generalized to qudits [29], and although experimental manipulations are more challenging for these systems, significant progress [30–41] in qudit control has been made, and it has also been numerically shown that a larger qudit dimension can lead to an increased, more tolerant error correction threshold [42–47].

Most studies of stabilizer error correction codes focus on incoherent Pauli errors [48], considering their classical simulability [49] and justified by the discretization of errors by stabilizer measurements [1,4,50]. However, increasing technological precision has motivated the study of more realistic error models in qubit codes [48,51–61]. Broader classes of channels that can be classically efficiently simulated have been investigated [62–64], and the Pauli twirling approximation (PTA) turns out to be a practical approach to mapping the non–Pauli error channel to the code-compatible Pauli model [65–73]. Despite the effort in qubit codes, general error models for qudit codes have received less attention [74], and the implementation of qudit Pauli twirling [75,76] requires a larger set of twirling gates as the dimension d of the qudit increases, making it operationally difficult. Moreover, it has been shown that in both transmon qutrit [34,35,40] and trapped ion qudit [77,78] systems the naturally occurring errors are not the cyclic shifts described by the most common generalization of the Pauli matrices. These considerations call into question the benefit of explicitly applying the Pauli twirling gates, and lead us to ask, to what extent can non–Pauli error models be investigated, such that their intrinsic correlations may be leveraged to improve the codes?

In this Letter, we study the qudit 2D square lattice surface code, where each physical qudit is subject to a stochastic non–Pauli error channel. By classifying the error subgraphs [79–81], inspired by belief propagation [82,83], we connect the remaining correlations removed in the PTA with the distribution of loop sizes in Bernoulli percolation theory [84]. We find that for a physical error rate below the qudit error correction threshold, with an upper limit estimated at 30% [43], the partially discretized coherent errors are sparse and mostly involve only four neighboring qudits, while the largest spatial span of their correlation is local, growing only logarithmically with the code distance. As the computational complexity depends exponentially on the span of these correlations, the strong localization observed implies that explicitly keeping track of correlations remains numerically efficient. Our findings, independent of dimension and the specific forms of the non–Pauli errors, justify the possibility of efficiently exploring qudit code performances beyond Pauli error models.

Surface code error discretization.—Consider the two-dimensional surface code with d-dimensional qudits on a square lattice [45], with size characterized by the two parameters n_h and n_v. An example is shown in Fig. 1. On the primal lattice, the vertical (horizontal) boundaries are smooth (rough). For later convenience when dealing with deformed stabilizers at the boundaries and logical operators, we contract all the nodes on rough boundaries into a

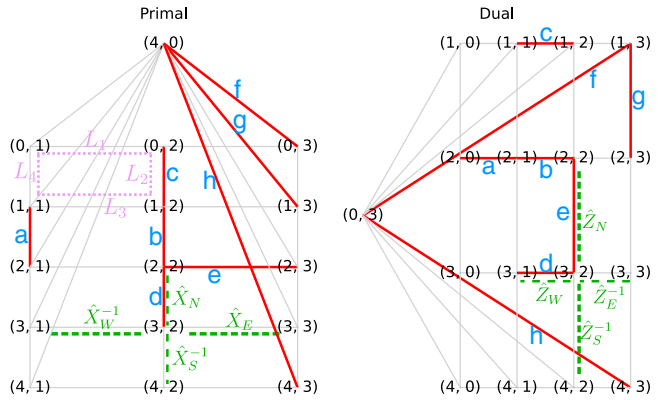

FIG. 1. An example 2D surface code with $n_h = 4$ and $n_v = 5$. On the primal lattice, the horizontal (vertical) size n_h (n_v) refers to the number of edges (nodes) in each row (column). Qudits subject to the error $\hat{F}$ are marked in thick red lines and labeled by blue letters. An example of a vertex (plaquette) operator is shown on the primal (dual) lattice centered at the node (3,2) [(3,2)], where relevant qudits on the edges are marked by green dashed lines and the Pauli operators are labeled in green. An example loop is shown in pink dotted lines, with the qudits labeled as $L_1 \to L_4$.

single dummy node. The d-dimensional Pauli operators are $\hat{X} = \sum_{j=0}^{d-1} |j \oplus 1\rangle\langle j|$ and $\hat{Z} = \sum_{j=0}^{d-1} \omega^j |j\rangle\langle j|$, where $\oplus$ is the sum modulo d and $\omega = \exp(i2\pi/d)$. They satisfy the commutation relation $\hat{X}^j\hat{Z}^k = \omega^{-jk}\hat{Z}^k\hat{X}^j$. Stabilizer generators are vertex operators in the Pauli-X basis and plaquette operators in the Pauli-Z basis, though for our purposes the Z-basis stabilizers are better viewed as vertex operators on the dual lattice.

As the simplest functioning model, we assume a quantum channel $\mathcal{L}_s$ for each qudit,

$$\mathcal{L}_s(\rho) = (1-p)\rho + p\hat{F}\rho\hat{F}^\dagger, \quad \text{with} \quad \hat{F} = \sum_{i,j=0}^{d-1} f_{i,j}\hat{X}^i\hat{Z}^j, \tag{1}$$

where each qudit experiences a general unitary error $\hat{F}$ with probability p. This operator can be decomposed into a linear sum of Pauli operators, as $\{\hat{X}^i\hat{Z}^j\}$ forms the complete Heisenberg-Weyl basis [85]. This model can be straightforwardly generalized to a mixture of single-qudit errors applying some $\hat{F}^{(k)}$ with probability p_k, which are not necessarily unitary. It can even allow different errors for each qudit. These types of models incorporate noncyclic transitions between different levels in a qudit. In the Supplemental Material [86], we give physical examples involving nonunitary $\hat{F}$ operators, to emphasize the importance of going beyond stochastic Pauli errors.

An example error pattern is shown in Fig. 1, where the erroneous qudit edges are marked in red and labeled $a \to h$. These edges induce the *error subgraph*. For each error pattern, syndrome measurements project the erroneous state into a subspace compatible with a specific syndrome [4]. As the syndrome subspace is constructed via Pauli operators acting on the code space, we expand the product of $\hat{F}$ operators into a sum of multiqudit Pauli operators. Importantly, if two multiqudit Pauli operators bring the logical state into the same syndrome subspace, the probability of being projected into this subspace will depend on interference between the complex amplitudes $f_{i,j}$. This effect, absent under the PTA, increases the computational complexity of numerically sampling the syndrome, and appears when the error pattern can lead to the formation of a stabilizer or a logical operator. Whether or not this effect exists can be determined from the graph classification of the contracted lattice (e.g., Fig. 1). Specifically, for each error pattern, if the error subgraphs on both the contracted primal and dual lattices are forests, the syndrome measurements fully discretize the errors in the Pauli basis. A *forest* is a graph that contains no loops, and each connected component in a forest is a *tree* [79,80]. For example, in the primal lattice in Fig. 1, the error subgraph contains three trees: $\{a\}$, $\{b, c, d, e\}$, and $\{f, g, h\}$. Complete discretization of errors in the Pauli basis suggests that the error channel can be replaced by the Pauli twirled channel,

$$\tilde{\mathcal{L}}_s(\rho) = \frac{1}{d^2}\sum_{i,j=0}^{d-1} \hat{Z}^{-j}\hat{X}^{-i}\mathcal{L}_s(\hat{X}^i\hat{Z}^j\rho\hat{Z}^{-j}\hat{X}^{-i})\hat{X}^i\hat{Z}^j, \tag{2}$$

whose effect is to keep only the diagonal terms in $\hat{F}\rho\hat{F}^\dagger$. Importantly, this equivalence only relies on the relative positions of the erroneous qudits, and is independent of the qudit dimension d and the specific values of $f_{i,j}$ in $\hat{F}$. From an operational perspective, this equivalence implies that for forest error subgraphs the computational complexity is the same as that of the PTA channel Eq. (2).

On the contrary, PTA breaks down if loops are formed. While edges that do not form part of a loop can be fully discretized, errors on loop edges can only be partially discretized in the Pauli basis. Consider a loop, for example, consisting of qudits $L_1 \to L_4$ marked in pink dashed lines in Fig. 1. The error $\hat{F}_{L_1}\hat{F}_{L_2}\hat{F}_{L_3}\hat{F}_{L_4}$ can be expanded as a sum over products of Pauli operators, which contains the stabilizer operator $\hat{S}_p = \hat{Z}_{L_1}\hat{Z}_{L_2}^{-1}\hat{Z}_{L_3}^{-1}\hat{Z}_{L_4}$ and all of its powers $\hat{S}_p^k$ for $k = 0, 1, \ldots, d-1$. Products of Pauli errors that differ only by a power of $\hat{S}_p$ correspond to the same syndrome: The probability of projection into the compatible subspace differs from the PTA due to the interference of complex amplitudes $f_{i,j}$ on the loop. For each connected component in the error subgraph, the numerical cost is expected to increase with d^l, where l is the tree width of the component [92–94]. We can therefore study the increase in sampling complexity by quantifying the number and size of loops in the error subgraph, independent of the specific form of the error $\hat{F}$. Once the syndrome is sampled, Pauli operators compatible with the syndrome are applied to

recover the logical state and decoders developed for Pauli error models can be applied.

In the Supplemental Material [86], we provide examples of how the state evolves under measurement, demonstrating how the sampling complexity increases with the tree-width and how belief propagation is applied.

Relation to percolation theory.—The 2D surface code modeled above can be directly mapped into the problem of Bernoulli percolation [95] on the square lattice, which is a bond percolation model [96] where each edge is retained only with probability p, independent of other edges. Bernoulli percolation has been extensively studied, and size distributions for clusters (connected components of the error subgraph) have been investigated both above and below the critical probability $p_c = 0.5$ [84,97]. In the subcritical regime, for instance, the mean size of the largest connected cluster has been found to scale logarithmically with the total number of edges. However, to the best of our knowledge only at the percolation threshold [98–102] has the distribution of loops been studied [81,99]. We are interested in this distribution below the error correction threshold [43], which is in the subcritical percolation regime. We use two measures to infer the loop size distribution. The first is the proportion of error subgraph edges that are loop edges, which quantifies how likely loops are to form (scaling with p also providing information on the mean size). The second measure is the maximal one-dimensional span of a loop. This quantifies the size of the largest loop, in contrast to the mean, that can form in the subcritical lattice.

Proportion of loop-edges.—We first consider the ratio between the number of qudits associated with loop edges on the error subgraphs and the total number of erroneous qudits, denoted $p_{\text{loop-edge}}$. We use Monte Carlo simulations, finding a cycle basis in the error subgraph [103,104] for each sampled error pattern on the primal lattice. This process is repeated for the dual lattice, removing redundancies where a qudit is involved in loops on both lattices and taking the sample average.

We can obtain an approximate analytical formula for $p_{\text{loop-edge}}$. Below the percolation threshold, the dominant contributions come from the smallest loops, which include the three-edge loops on the rough boundaries and the four-edge loops inside the bulk of each lattice. The primal [or dual] lattice has $2(n_v - 1)$ [or $2(n_h - 1)$] three-edge loops, each appearing with probability roughly p^3, and $(n_h - 2)(n_v - 1)$ [or $(n_h - 1)(n_v - 2)$] four-edge loops, each appearing with probability roughly p^4. We obtain

$$p_{\text{loop-edge}} \approx 3\frac{n_h + n_v}{n_h n_v} p^2 + 4p^3. \tag{3}$$

The first part of Eq. (3) describes the dependence of $p_{\text{loop-edge}}$ on the size and shape of the surface code, which matters more for smaller lattices. The second part only depends on p, capturing the asymptotic behavior for larger lattices. In Fig. 2, we show the value of $p_{\text{loop-edge}}$ as a function of n_h, for the most symmetric shapes, $n_h = n_v \pm 1$.

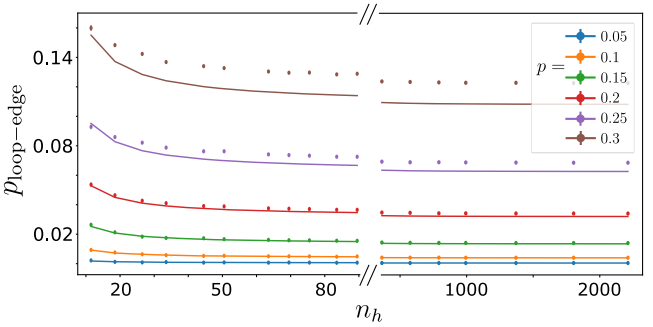

FIG. 2. The proportion of erroneous qudits in loops as a function of the lattice size n_h, for near-symmetric lattices $n_h = n_v \pm 1$. Colors correspond to different single qudit physical error rates. Solid lines follow the analytical expression Eq. (3). Markers are from the Monte Carlo simulations, and error bars represent the standard deviation. The left (right) half of the figure shows the behavior for smaller (larger) values of n_h, for a Monte Carlo sample size of 2000 (200).

The analytical expression Eq. (3) fits well with the numerical simulation result for $p \leq 0.2$, but for larger p the analytical formula underestimates $p_{\text{loop-edge}}$. This implies that the contribution from larger loops becomes non-negligible as p increases. We consider a correction term in place of the $4p^3$ term in Eq. (3). As plotted in Fig. 3, for the four pairs of (n_h, n_v) in the asymptotic regime, the linear functions of $\log(p_{\text{loop-edge}})$ versus $\log(p)$ are very similar. This verifies the approximate shape independence of $p_{\text{loop-edge}}$, and indicates that we may take the simulation result of the surface code with the maximum number of physical qudits, which is panel (c) in Fig. 3, to define the correction as $4.745p^{3.057}$ that replaces $4p^3$ in Eq. (3). The exponent 3.057 implies that for $p > 0.2$, though the average loop size is slightly larger than 4, most of the correlations remain tightly constrained to the smallest local loops.

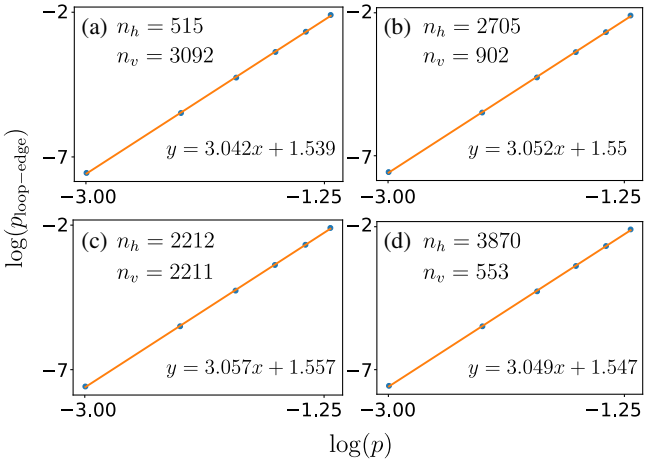

FIG. 3. Linear fitting of $y = \log(p_{\text{loop-edge}})$ as a function of $x = \log(p)$ for four different lattice sizes. Blue markers are for the numerical data from the Monte Carlo simulations, while orange lines are the results of the fitting (expressions shown).

We have also numerically verified that the difference between the analytical and numerical results of $p_{\text{loop-edge}}$ can be compensated if instead of the linear fitting, we add a term $6p^5$ to the analytical expression Eq. (3). This implies that in addition to the dominant four-edged loops, a non-negligible number of six-edged loops appear in the error subgraph. Connected components with loops of at most four and six edges both have tree width $l = 2$. Based on this modified expression for $p_{\text{loop-edge}}$, we can deduce that they appear approximately $2n_h n_v p^4$ and $2n_h n_v p^6$ times, respectively, for each error pattern. As a result, the increased time complexity due to residual correlations is expected to be $O[2n_h n_v(p^4 + p^6)d^2]$. This is polynomial in both the code distance and the qudit dimension with power 2, indicating that numerical sampling remains efficient for lattices of the sizes considered, with n_h into the thousands. There might be more four-edge loops as a result of correlated errors induced during stabilizer measurements. These are, however, expected to be on the same order as the number of four-edge loops already described, so that the order of magnitude for the sampling complexity should not change.

In the Supplemental Material [86], we demonstrate the dependence of $p_{\text{loop-edge}}$ on the aspect ratio n_h/n_v. We also describe a binary criterion based on the simple presence or absence of loops, which is useful for bounding the accuracy of logical error rate estimates for small lattices.

Maximal one-dimensional span of a loop.—The proportion of loop edges considered above describes average behavior. Taking a different perspective, we next estimate the maximal loop size, putting an upper bound on the span of the correlations. Specifically, for each loop we take the one-dimensional span, this being the maximal length of its smallest bounding rectangle. For example, for the four-edged elementary loop considered above, the span is 1. The maximum span over all loops on both the primal and the dual lattices is our target value, $L_{\text{max,loop}}$.

In Fig. 4, we show the numerical result of how $L_{\text{max,loop}}$ behaves as a function of n_h for symmetric lattices, on linear and logarithmic scales. As n_h increases, $L_{\text{max,loop}}$ also increases but at a much slower rate. The straight lines, especially for larger values of p, indicate that the maximal one-dimensional span of a loop grows logarithmically with the lattice size. This scaling is similar to the finding in percolation theory that below the percolation threshold, the maximal cluster size increases logarithmically [84], though the full cluster also includes nonloop edges. Our finding focusing on loops only thus supplements the scaling behaviors in percolation theory.

As $L_{\text{max,loop}} + 1$ bounds the maximal tree width of a cluster, its logarithmic scaling with respect to n_h indicates that the sampling complexity scales at most polynomially in the lattice size. As shown in Fig. 4, up to $n_h = 2 \times 10^3$ and $p = 0.3$, this complexity is on the order of d^9 as $L_{\text{max,loop}} \approx 8$. While the exponent increases very slowly with n_h, we do observe a rapid increase with p. It was

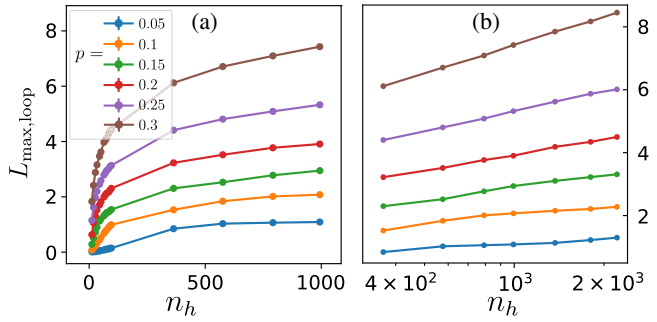

FIG. 4. The maximal one-dimensional span of a loop as a function of the lattice size n_h for almost symmetric lattices $n_h = n_v \pm 1$. Points are obtained via Monte Carlo simulation with 2000 samples, and error bars represent the standard deviation. Colors correspond to different single qudit physical error rates. (a) Linear scale. (b) Logarithmic scale.

shown in Ref. [43] that $p = 0.3$ corresponds to the accuracy threshold in the limit $d \to \infty$, while for more practical values of d the threshold will be closer to $p = 0.2$. Therefore, for numerical investigations of qudit surface code thresholds we expect an upper bound on the sampling complexity closer to d^5 as $L_{\text{max,loop}} \approx 4$.

In the Supplemental Material [86] we use another measure for the maximum loop size, the total number of nodes in a loop, with similar behavior to Fig. 4(a). We also show that due to the slow increase of $L_{\text{max,loop}}$ with n_h, lattice asymmetry has little effect.

Conclusion.—In this Letter, identifying that residual multiqudit correlations in topological codes are restricted to cell boundaries (or loops, in two dimensions) of the error subgraph, we assess the complexity of syndrome sampling in qudit surface codes under stochastic single-qudit non-Pauli errors from the perspectives of cycle detection and percolation theory. Our analysis is independent of the qudit dimension and the specific form of the errors.

Considering a single-qudit physical error rate p up to 30% (the highest threshold predicted in qudit surface codes [43]), we quantify the average and maximal error loop sizes. We find that the former, which as a mean value is related to the run time of the code simulation, is well modeled accounting only for four-edged loops plus a small correction from six-edged loops on the order of p^2, both of which have tree width 2. The latter, which as an upper bound is related to the maximal memory required, grows only logarithmically with the code size n_h, dropping rapidly as p decreases, and up to $n_h = 2000$ and $p = 0.3$ gives an upper bound of 9 for the tree width.

The efficient scaling observed in our results indicates that syndrome sampling complexity does not prevent the inclusion of non–Pauli errors; the complexity of the decoding step is expected to remain the limiting factor. An investigation of qudit surface codes under general stochastic errors is therefore within reach. Intrinsic correlations may be leveraged to improve the codes, especially for $d > 2$ qudit

systems that have a richer structure than the biased error models of qubit systems. We thus expect our results to motivate further investigation of qudit surface codes, where the less widely studied physical channels acting between multiple native levels may be found to have advantages over more restrictive Pauli-twirled two-level systems.

By taking into account other percolation structures, our method may also be generalized beyond a single-qudit error model, and even to multiqudit coherent errors [53], where the discretization of errors by stabilizer measurements appears also as a central step.

We acknowledge financial support from the Samsung GRC project, the UK Hub in Quantum Computing and Simulation with funding from UKRI EPSRC Grant No. EP/T001062/1, EPSRC Distributed Quantum Computing and Applications Grant No. EP/W032643/1, and the UK National Quantum Hub for Imaging (QUANTIC, No. EP/T00097X/1).

[1] P. W. Shor, Phys. Rev. A **52**, R2493 (1995).
[2] A. R. Calderbank and P. W. Shor, Phys. Rev. A **54**, 1098 (1996).
[3] A. Steane, Proc. R. Soc. A **452**, 2551 (1996).
[4] R. Raussendorf, Phil. Trans. R. Soc. A **370**, 4541 (2012).
[5] E. T. Campbell, B. M. Terhal, and C. Vuillot, Nature (London) **549**, 172 (2017).
[6] S. M. Girvin, arXiv:2111.08894.
[7] S. B. Bravyi and A. Y. Kitaev, arXiv:quant-ph/9811052.
[8] E. Dennis, A. Kitaev, A. Landahl, and J. Preskill, J. Math. Phys. (N.Y.) **43**, 4452 (2002).
[9] A. Y. Kitaev, Ann. Phys. (Amsterdam) **303**, 2 (2003).
[10] M. H. Freedman and D. A. Meyer, Found. Comput. Math. **1**, 325 (2001).
[11] D. S. Wang, A. G. Fowler, and L. C. Hollenberg, Phys. Rev. A **83**, 020302 (2011).
[12] A. G. Fowler, M. Mariantoni, J. M. Martinis, and A. N. Cleland, Phys. Rev. A **86**, 032324 (2012).
[13] A. M. Stephens, Phys. Rev. A **89**, 022321 (2014).
[14] B. M. Terhal, Rev. Mod. Phys. **87**, 307 (2015).
[15] R. Barends, J. Kelly, A. Megrant, A. Veitia, D. Sank, E. Jeffrey, T. C. White, J. Mutus, A. G. Fowler, B. Campbell *et al.*, Nature (London) **508**, 500 (2014).
[16] D. Nigg, M. Mueller, E. A. Martinez, P. Schindler, M. Hennrich, T. Monz, M. A. Martin-Delgado, and R. Blatt, Science **345**, 302 (2014).
[17] J. Kelly, R. Barends, A. G. Fowler, A. Megrant, E. Jeffrey, T. C. White, D. Sank, J. Y. Mutus, B. Campbell, Y. Chen *et al.*, Nature (London) **519**, 66 (2015).
[18] A. D. Córcoles, E. Magesan, S. J. Srinivasan, A. W. Cross, M. Steffen, J. M. Gambetta, and J. M. Chow, Nat. Commun. **6**, 6979 (2015).
[19] M. Takita, A. D. Córcoles, E. Magesan, B. Abdo, M. Brink, A. Cross, J. M. Chow, and J. M. Gambetta, Phys. Rev. Lett. **117**, 210505 (2016).
[20] A. Erhard, H. Poulsen Nautrup, M. Meth, L. Postler, R. Stricker, M. Stadler, V. Negnevitsky, M. Ringbauer, P. Schindler, H. J. Briegel *et al.*, Nature (London) **589**, 220 (2021).
[21] Z. Chen, K. J. Satzinger, J. Atalaya, A. N. Korotkov, A. Dunsworth, D. Sank, C. Quintana, M. McEwen, R. Barends, P. V. Klimov *et al.*, Nature (London) **595**, 383 (2021).
[22] J. Marques, B. Varbanov, M. Moreira, H. Ali, N. Muthusubramanian, C. Zachariadis, F. Battistel, M. Beekman, N. Haider, W. Vlothuizen *et al.*, Nat. Phys. **18**, 80 (2022).
[23] S. Krinner, N. Lacroix, A. Remm, A. Di Paolo, E. Genois, C. Leroux, C. Hellings, S. Lazar, F. Swiadek, J. Herrmann *et al.*, Nature (London) **605**, 669 (2022).
[24] Y. Zhao, Y. Ye, H.-L. Huang, Y. Zhang, D. Wu, H. Guan, Q. Zhu, Z. Wei, T. He, S. Cao *et al.*, Phys. Rev. Lett. **129**, 030501 (2022).
[25] S. S. Bullock, D. P. O'Leary, and G. K. Brennen, Phys. Rev. Lett. **94**, 230502 (2005).
[26] A. Bocharov, M. Roetteler, and K. M. Svore, Phys. Rev. A **96**, 012306 (2017).
[27] A. Pavlidis and E. Floratos, Phys. Rev. A **103**, 032417 (2021).
[28] E. Gustafson, arXiv:2201.04546.
[29] S. S. Bullock and G. K. Brennen, J. Phys. A **40**, 3481 (2007).
[30] B. P. Lanyon, T. J. Weinhold, N. K. Langford, J. L. O'Brien, K. J. Resch, A. Gilchrist, and A. White, Phys. Rev. Lett. **100**, 060504 (2008).
[31] R. Bianchetti, S. Filipp, M. Baur, J. M. Fink, C. Lang, L. Steffen, M. Boissonneault, A. Blais, and A. Wallraff, Phys. Rev. Lett. **105**, 223601 (2010).
[32] J. Wang, S. Paesani, Y. Ding, R. Santagati, P. Skrzypczyk, A. Salavrakos, J. Tura, R. Augusiak, L. Mančinska, D. Bacco *et al.*, Science **360**, 285 (2018).
[33] M. Ringbauer, T. R. Bromley, M. Cianciaruso, L. Lami, W. S. Lau, G. Adesso, A. G. White, A. Fedrizzi, and M. Piani, Phys. Rev. X **8**, 041007 (2018).
[34] M. S. Blok, V. V. Ramasesh, T. Schuster, K. O'Brien, J.-M. Kreikebaum, D. Dahlen, A. Morvan, B. Yoshida, N. Y. Yao, and I. Siddiqi, Phys. Rev. X **11**, 021010 (2021).
[35] A. Morvan, V. Ramasesh, M. Blok, J. Kreikebaum, K. O'Brien, L. Chen, B. Mitchell, R. Naik, D. Santiago, and I. Siddiqi, Phys. Rev. Lett. **126**, 210504 (2021).
[36] M. A. Yurtalan, J. Shi, M. Kononenko, A. Lupascu, and S. Ashhab, Phys. Rev. Lett. **125**, 180504 (2020).
[37] M. Ringbauer, M. Meth, L. Postler, R. Stricker, R. Blatt, P. Schindler, and T. Monz, Nat. Phys. **18**, 1053 (2022).
[38] Y. Chi, J. Huang, Z. Zhang, J. Mao, Z. Zhou, X. Chen, C. Zhai, J. Bao, T. Dai, H. Yuan *et al.*, Nat. Commun. **13**, 1 (2022).
[39] P. Hrmo, B. Wilhelm, L. Gerster, M. W. van Mourik, M. Huber, R. Blatt, P. Schindler, T. Monz, and M. Ringbauer, Nat. Commun. **14**, 2242 (2023).
[40] N. Goss, A. Morvan, B. Marinelli, B. K. Mitchell, L. B. Nguyen, R. K. Naik, L. Chen, C. Jünger, J. M. Kreikebaum, D. I. Santiago *et al.*, Nat. Commun. **13**, 7841 (2022).
[41] T. Roy, Z. Li, E. Kapit, and D. I. Schuster, arXiv:2211.06523.
[42] G. Duclos-Cianci and D. Poulin, Phys. Rev. A **87**, 062338 (2013).
[43] H. Anwar, B. J. Brown, E. T. Campbell, and D. E. Browne, New J. Phys. **16**, 063038 (2014).

[44] R. S. Andrist, J. R. Wootton, and H. G. Katzgraber, Phys. Rev. A **91**, 042331 (2015).
[45] F. H. Watson, H. Anwar, and D. E. Browne, Phys. Rev. A **92**, 032309 (2015).
[46] A. Hutter, D. Loss, and J. R. Wootton, New J. Phys. **17**, 035017 (2015).
[47] J. Marks, T. Jochym-O'Connor, and V. Gheorghiu, New J. Phys. **19**, 113022 (2017).
[48] T. R. Scruby, M. Vasmer, and D. E. Browne, Phys. Rev. Research **4**, 043052 (2023).
[49] D. Gottesman, arXiv:quant-ph/9807006.
[50] M. A. Nielsen and I. L. Chuang, *Quantum Computation and Quantum Information: 10th Anniversary Edition* (Cambridge University Press, Cambridge, England, 2010).
[51] J. Ghosh, A. G. Fowler, and M. R. Geller, Phys. Rev. A **86**, 062318 (2012).
[52] A. S. Darmawan and D. Poulin, Phys. Rev. Lett. **119**, 040502 (2017).
[53] S. Bravyi, M. Englbrecht, and R. König, and N. Peard, npj Quantum Inf. **4**, 55 (2018).
[54] S. J. Beale, J. J. Wallman, M. Gutiérrez, K. R. Brown, and R. Laflamme, Phys. Rev. Lett. **121**, 190501 (2018).
[55] E. Huang, A. C. Doherty, and S. Flammia, Phys. Rev. A **99**, 022313 (2019).
[56] J. K. Iverson and J. Preskill, New J. Phys. **22**, 073066 (2020).
[57] F. Venn and B. Béri, Phys. Rev. Res. **2**, 043412 (2020).
[58] J. P. Bonilla Ataides, D. K. Tuckett, S. D. Bartlett, S. T. Flammia, and B. J. Brown, Nat. Commun. **12**, 2172 (2021).
[59] K. Tiurev, P.-J. H. Derks, J. Roffe, J. Eisert, and J.-M. Reiner, arXiv:2208.02191.
[60] E. Novais and E. R. Mucciolo, Phys. Rev. Lett. **110**, 010502 (2013).
[61] B. J. Brown, D. Loss, J. K. Pachos, C. N. Self, and J. R. Wootton, Rev. Mod. Phys. **88**, 045005 (2016).
[62] E. Magesan, D. Puzzuoli, C. E. Granade, and D. G. Cory, Phys. Rev. A **87**, 012324 (2013).
[63] M. Gutiérrez, L. Svec, A. Vargo, and K. R. Brown, Phys. Rev. A **87**, 030302 (2013).
[64] D. Puzzuoli, C. Granade, H. Haas, B. Criger, E. Magesan, and D. G. Cory, Phys. Rev. A **89**, 022306 (2014).
[65] M. Silva, E. Magesan, D. W. Kribs, and J. Emerson, Phys. Rev. A **78**, 012347 (2008).
[66] M. R. Geller and Z. Zhou, Phys. Rev. A **88**, 012314 (2013).
[67] Y. Tomita and K. M. Svore, Phys. Rev. A **90**, 062320 (2014).
[68] M. Gutiérrez and K. R. Brown, Phys. Rev. A **91**, 022335 (2015).
[69] A. Katabarwa and M. R. Geller, Sci. Rep. **5**, 1 (2015).
[70] A. Katabarwa, arXiv:1701.03708.
[71] M. Gutiérrez, C. Smith, L. Lulushi, S. Janardan, and K. R. Brown, Phys. Rev. A **94**, 042338 (2016).
[72] Z. Cai and S. C. Benjamin, Sci. Rep. **9**, 11281 (2019).
[73] J. E. Martinez, P. Fuentes, P. M. Crespo, and J. Garcia-Frias, IEEE Access **8**, 172623 (2020).
[74] M. Grassl, L. Kong, Z. Wei, Z.-Q. Yin, and B. Zeng, IEEE Trans. Inf. Theory **64**, 4674 (2018).
[75] M. Jafarzadeh, Y.-D. Wu, Y. R. Sanders, and B. C. Sanders, New J. Phys. **22**, 063014 (2020).
[76] A. Goswami, M. Mhalla, and V. Savin, in *2021 IEEE International Symposium on Information Theory (ISIT)* (IEEE, New York, 2021), pp. 1487–1492.
[77] A. Klimov, R. Guzmán, J. Retamal, and C. Saavedra, Phys. Rev. A **67**, 062313 (2003).
[78] P. J. Low, B. M. White, A. A. Cox, M. L. Day, and C. Senko, Phys. Rev. Res. **2**, 033128 (2020).
[79] R. Diestel, *Graph Theory* (Springer, Berlin, Heidelberg, 2017).
[80] A. Bondy and U. Murty, *Graph Theory* (Springer, London, 2010).
[81] X. Xu, J. Wang, Z. Zhou, T. M. Garoni, and Y. Deng, Phys. Rev. E **89**, 012120 (2014).
[82] J. Pearl, in *Probabilistic and Causal Inference: The Works of Judea Pearl*, edited by H. Geffner, R. Dechter, and J. Y. Halpern (Association for Computing Machinery, New York, NY, United States, 2022), pp. 129–138.
[83] J. H. Kim and J. Pearl, in *Proceedings of the Eighth international joint conference on Artificial intelligence* (Morgan Kaufmann Publishers Inc., 1983), pp. 190–193.
[84] M. Z. Bazant, Phys. Rev. E **62**, 1660 (2000).
[85] A. Asadian, P. Erker, M. Huber, and C. Klöckl, Phys. Rev. A **94**, 010301 (2016).
[86] See Supplemental Material at http://link.aps.org/supplemental/10.1103/PhysRevLett.131.200602, which covers generalization and physical correspondence of the stochastic non-Pauli noise models, explicit examples of discretizing the errors by stabilizer measurements, probability of not equivalent to the Pauli-twirled channel, dependence of the proportion of erroneous qudits that are in loops on the lattice asymmetry, maximal one-dimensional span of a loop for asymmetric lattices and maximal total number of nodes in a loop, and includes Refs. [87–91].
[87] J. Pearl, in *Proceedings of the Second AAAI Conference on Artificial Intelligence* (AAAI Press, Pittsburgh, 1982), pp. 133–136.
[88] Y. Wang, M. Um, J. Zhang, S. An, M. Lyu, J.-N. Zhang, L.-M. Duan, D. Yum, and K. Kim, Nat. Photonics **11**, 646 (2017).
[89] K. Georgopoulos, C. Emary, and P. Zuliani, Phys. Rev. A **104**, 062432 (2021).
[90] C. Blank, D. K. Park, J.-K. K. Rhee, and F. Petruccione, npj Quantum Inf. **6**, 41 (2020).
[91] D. Mc Hugh and J. Twamley, New J. Phys. **7**, 174 (2005).
[92] N. Robertson and P. Seymour, J. Algorithms **7**, 309 (1986).
[93] F. V. Jensen, S. L. Lauritzen, and K. G. Olesen, Computational statistics quarterly : CSQ **4**, 269 (1990), physica-Verlag.
[94] I. L. Markov and Y. Shi, SIAM J. Comput. **38**, 963 (2008).
[95] H. Duminil-Copin, in *Proceedings of the International Congress of Mathematicians: Rio de Janeiro 2018* (World Scientific, Singapore, 2018), pp. 2829–2856.
[96] D. Stauffer and A. Aharony, *Introduction to Percolation Theory* (Taylor & Francis, London, 2018).
[97] P. Grinchuk, Phys. Rev. E **66**, 016124 (2002).
[98] H. E. Stanley, J. Phys. A **10**, L211 (1977).
[99] H. J. Herrmann and H. E. Stanley, Phys. Rev. Lett. **53**, 1121 (1984).

[100] M. F. Gyure, M. V. Ferer, B. F. Edwards, and G. Huber, Phys. Rev. E **51**, 2632 (1995).
[101] A. Bunde and W. Dieterich, J. Electroceram. **5**, 81 (2000).
[102] Z. He and H. Hu, Physica (Amsterdam) **570A**, 125806 (2021).
[103] A. A. Hagberg, D. A. Schult, and P. J. Swart, in *Proceedings of the 7th Python in Science Conference*, edited by G. Varoquaux, T. Vaught, and J. Millman (Pasadena, CA USA, 2008), pp. 11–15.
[104] K. Paton, Commun. ACM **12**, 514 (1969).